Applied Physics Letters ARTICLE scitation.org/journal/apl

One-dimensional bandgap modulation at continuous few-layer MoS_2 steps

Cite as: Appl. Phys. Lett. **121**, 233103 (2022); doi: 10.1063/5.0117436
Submitted: 1 August 2022 · Accepted: 23 November 2022 ·
Published Online: 9 December 2022

View Online Export Citation CrossMark

Yu-Hsun Chu,[1] Hou-Ju Chen,[1] Shin-Ye Lee,[1] Christopher John Butler,[1] Li-Syuan Lu,[2] Han Yeh,[2] Wen-Hao Chang,[2,3,4] and Minn-Tsong Lin[1,4,5,a)]

AFFILIATIONS

[1]Department of Physics, National Taiwan University, Taipei 10617, Taiwan
[2]Department of Electrophysics, National Chiao Tung University, Hsinchu 30013, Taiwan
[3]Taiwan Consortium of Emergent Crystalline Materials (TCECM), Ministry of Science and Technology, Taipei 10622, Taiwan
[4]Research Center for Applied Sciences, Academia Sinica, Taipei 11529, Taiwan
[5]Institute of Atomic and Molecular Sciences, Academia Sinica, Taipei 10617, Taiwan

[a)]**Author to whom correspondence should be addressed:** mtlin@phys.ntu.edu.tw

ABSTRACT

In pursuit of novel two-dimensional devices, lateral heterostructures based on transition metal dichalcogenides (TMDCs) have been intensively proposed and demonstrated. For instance, heterojunctions composed of TMDCs with different thicknesses function attractively in electronics and optoelectronics. Using scanning tunneling microscopy and spectroscopy, we resolved electronic structures of three types of few-layer MoS_2 steps: flake edges, continuous bilayer–monolayer steps, and monolayers sitting on highly oriented pyrolytic graphite steps. Each type possesses unique bandgap features, including in-gap states and npn-like band alignment, which suggests modifiable 1D bandgaps via choices of edge conditions for the development of lateral TMDC devices.

Following the success of graphene,[1,2] monolayer transition metal dichalcogenides (TMDCs) MX_2 (M = W, Mo; X = S, Se) have stood out attracting wide attention in the recent decade.[3,4] Combinations of honeycomb structures, broken inversion symmetries, and strong spin–orbit coupling result in spin-split carrier valleys, which are of great importance to optoelectronics, spintronics, and valleytronics.[3,5] These two-dimensional (2D) direct-bandgap semiconductors have been widely applied to novel electronic devices.[6,7] In addition to appropriate bandgap widths and carrier mobility, the atomic thicknesses of 2D TMDCs allow a reduction in the gate length to the nanometer scale.

In the path toward 2D TMDC devices, modifications to the physical properties of the ultrathin TMDC flakes and the related heterostructures have been demonstrated.[8–11] In lateral heterostructures composed of flakes with different chemical compositions or thicknesses, intriguing carrier transport is expected across or along the 1D interfaces, at which enhancement of conductivity and photocurrents occurs.[12–16] These 2D heterostructures lead the exotic electronic bands to applications in lower dimensions. Among the studies of 1D interfaces, two typical geometries are assumed: stitching and open-edge steps. The first indicates two flakes stitched in the same plane, and the second indicates that the top layers terminate on the bottom ones and leave open edges. However, there exists a barely discussed type: a continuous step, in which the top layers cover the bottom layer edges smoothly. This continuous case also creates well-defined junction areas and allows modifications to electronic structures by adjusting the step condition.

In this article, we resolve variations of electronic structures at few-layer MoS_2 flake edges at the nanoscale. Both the continuous and discontinuous MoS_2 steps exist after the synthesis of multilayer flakes. Compared to bandgap reduction at the discontinuous upper layer edges in the bilayer and trilayer structures, the continuous bilayer–monolayer steps show intact semiconducting gaps and smooth npn-like band alignment. For comparison, monolayer MoS_2 sitting on bilayer-high HOPG (highly oriented pyrolytic graphite) steps is measured and shows less perturbed bandgaps despite similar geometries to the bilayer–monolayer MoS_2 steps. The unveiled band structure variety in few-layer MoS_2 steps suggests potential bandgap tuning via bottom-layer choices.

High-crystalline-quality multilayer MoS_2 flakes were grown directly on HOPG surfaces using the chemical vapor deposition (CVD) method. Cleaved HOPG was mounted on top of a ceramic boat with powder MoO_3 precursors inside at the downstream side of

the furnace, and another ceramic boat with powder sulfur precursors was set at the upper stream side at 170 °C. The center of the heating zone was kept at 750 °C with one Ar gas atmosphere. Volatile suboxide MoO_{3-x} appeared with increasing temperature, diffused onto the HOPG surface, and reacted with the sulfur vapor flow. The growth process took 10 min to achieve multilayer MoS_2 flakes before naturally cooling down to room temperature. Scanning tunneling microscopy (STM) and spectroscopy (STS) experiments were performed in *Omicron* multifunction chambers with a base pressure of 1×10^{-10} mbar at 77.8 K, at which energy resolution is around 26 meV. Before being transferred into the STM chamber, the sample was annealed at 200 °C for 2 h in ultrahigh vacuum to remove possible absorbates. STM images were acquired in the constant current mode, and STS was performed with the help of lock-in techniques with 15 mV bias modulation of the frequency of 800 Hz or numerical derivative of tunneling currents.

Our multilayer MoS_2 grown on HOPG are generally triangular islands with the appearance of pyramids or spirals (see the supplementary material), as the reported island growths of multilayer TMDCs.[17,18] Although mostly covered by MoS_2, small regions of the HOPG surfaces can be distinguished in STM images according to the lattice constant and the gapless STS feature. Using the HOPG surface as a reference, we can identify the layer numbers of respective MoS_2 areas.

In Fig. 1(a), the STM image shows a part of a multilayer MoS_2 flake, on which the number of layers is labeled. STS measurements were performed along the white dashed line in Fig. 1(a) to unveil variations of electronic structures across the steps. The spatially resolved STS map in Fig. 1(b) shows type-I band alignment with reduced bandgap widths in higher MoS_2 layers in agreement with reported calculations and measurements.[17,19,20] Both the conduction band minimum (CBM) and the valence band maximum (VBM) shift upwards at the step edges. While the CBM shifts around 0.2 eV at both edges, the VBM at the edges is about 0.9 and 0.5 eV higher than the bulk VBM in the bilayer and trilayer regions, respectively. The reduction in bandgap widths at the edges can be attributed to the presence of valence band in-gap states at the discontinuous MoS_2 edges.[12,13,21]

During growths, the MoS_2 islands expanded and occasionally overlapped each other, which created continuous steps. An illustration in Fig. 2(a) describes both the discontinuous and continuous cases. Along the direction pointed by an orange arrow, there exists a discontinuous terrace edge as the ones in Fig. 1. There also exists a step along the direction indicated by a white arrow, at which the top MoS_2 layer covers parts of the bottom layer edge. Different from the aforementioned discontinuous case, the same single layer smoothly transitions from the upper layer of a bilayer system into another monolayer, and thus, we call the step continuous.

In the STM image in Fig. 2(b), regions i and ii are bilayer, and regions iii and iv are monolayer. The inset in Fig. 2(b) shows superimposed fast Fourier transform (FFT) images of the atomic lattices acquired from individual STM images of each region. From the FFT image, it can be seen that there exists no relative rotation between regions i and ii, whereas the lattice orientations of regions i, iii, and iv are misaligned. As a result, the upper MoS_2 layer could be one single layer and the bottom layers belong to different MoS_2 flakes. Furthermore, steps i-to-iv and ii-to-iii are discontinuous, and steps between regions i and ii are continuous.

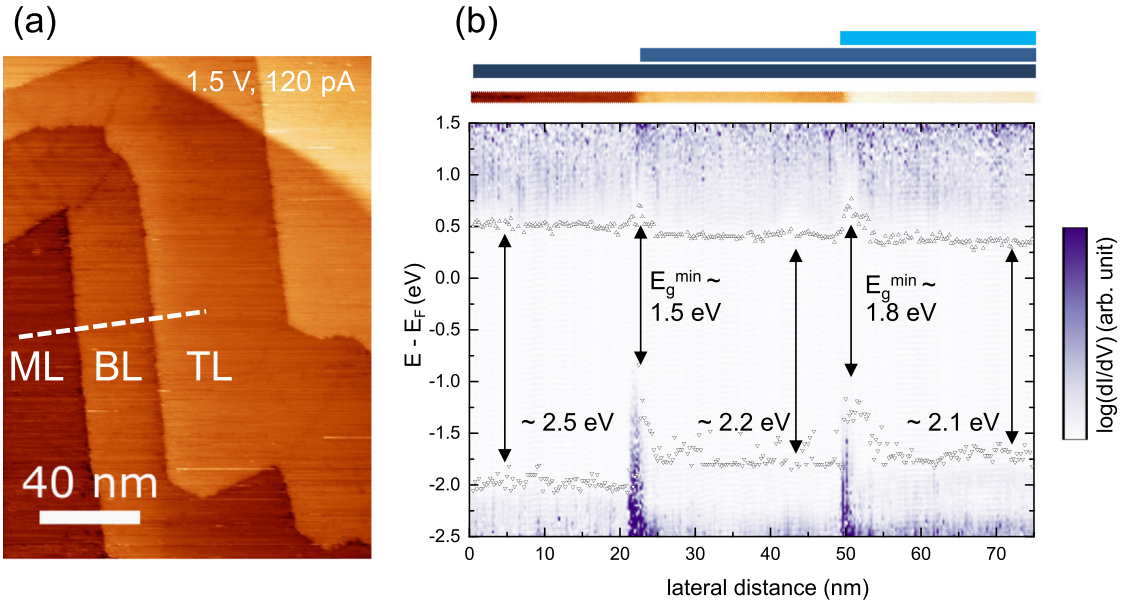

FIG. 1. (a) An STM image of multilayer MoS_2 on HOPG. The bottom-left corner is the first-layer MoS_2, and terraces above it are the second, the third, and so on. The first three layers are labeled ML (monolayer), BL (bilayer), and TL (trilayer). (b) An STS band diagram acquired along the white dashed line in (a) (set point: 1.5 V, 120 pA). Above the plot are a schematic drawing and an STM image taken with the STS measurements. Triangular dots are CBM and VBM obtained from curve fitting at each lateral position. The bandgap widths decrease from about 2.5 eV, 2.2 eV, to 2.1 eV for the monolayer, bilayer, and trilayer regions, respectively. The gap minimum at the edges is around 1.5 and 1.8 eV in the bilayer and trilayer steps.

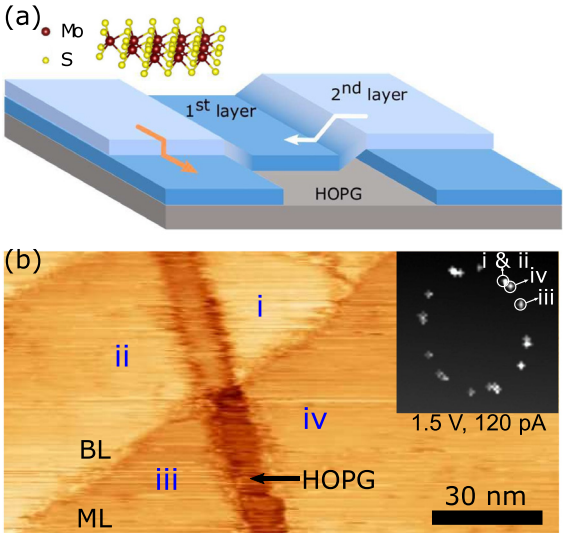

FIG. 2. (a) A sketch describing the continuous and discontinuous MoS_2 steps, which are marked by a white and an orange arrow, respectively. (b) An STM image of bilayer MoS_2 flakes. From the geometry and lattice orientations, regions i and ii are recognized as one single monolayer MoS_2 overlapping the other two monolayer flakes (regions iii and iv). Inset: superimposed fast Fourier transform of the atomic lattice of the four regions in the STM image.

Figure 3 shows band alignment acquired in the same manner as in the discontinuous case in Fig. 1. Band bending at both types of steps finishes within several nanometers from the step edges, which agrees with short depletion regions observed in studies of MoS_2 on graphene and HOPG.[12,13,22] The STS curves were measured with the tip cutting through the two continuous steps from region i to region ii in Fig. 2(b). The bulk bandgap widths are slightly smaller than the ones in Fig. 1(b), which could originate from differences in layer stacking and

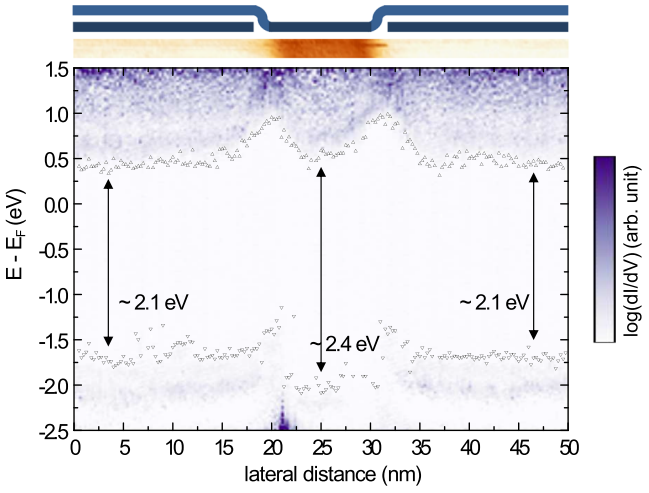

FIG. 3. An STS band diagram taken across two steps from region i to region ii in Fig. 2 (b), the corresponding topographic image, and a schematic illustration (set point: 1.5 V, 120 pA). The fitted CBM and VBM show bandgap widths around 2.4 and 2.1 eV for the monolayer and bilayer regions, respectively.

tip status. However, distinguishable features appear at the steps. Instead of gap reduction, the bandgap widths are close to the bulk values but the gap positions shift upwards. The energy shift is around 0.5 eV for the CBM and about 0.7 eV for the VBM compared to the bulk monolayer gaps. As a whole, the lateral bilayer–monolayer MoS_2 junction has an upward bandgap shift and an npn-like band alignment. The upward shift at the junction area could originate from band alignment and charge transfer in the top layer MoS_2 in close contact with the edge states. In close connection to the step edge and the edge states underneath, the top layer MoS_2 may experience band bending for alignment with the edge states, as the bulk-to-edge band bending.[13,21] The trapped states and dangling bonds can also induce dislocation-/substrate-induced charge transfer.[20,23,24] On the other hand, an opposite mechanism of flake detachment from the steps has been proposed for the lowered Fermi level of graphene at steps due to the suppression of electron doping from the substrates.[25] In the case of a continuous MoS_2 junction, detachment may lead to local quasi-free-standing monolayer regions with a larger bandgap and a higher gap position than the bilayer cases.[26,27]

To clarify the influences of substrate materials, we carried out STS measurements on monolayer MoS_2 on bilayer HOPG steps, as shown in Fig. 4(a). The apparent height of a bilayer HOPG step is around 0.7 nm, close to the height of monolayer MoS_2 flakes, so continuous MoS_2 steps with a similar geometry but a different bottom layer are created. Figure 4(b) shows no notable variations observed at the HOPG-induced MoS_2 steps. The VBM remains constant, and only a subtle upward shift of less than 0.1 eV appears in the CBM. All of the aforementioned bandgap variations are reproducible, and more STS diagrams are shown in the supplementary material.

Compared to the bandgap shift of more than 0.5 eV at the continuous bilayer–monolayer step, the barely disturbed bandgap at the HOPG-induced step unveils two features of the continuous MoS_2 steps. First, the bandgap properties depend on the choices of terraces under MoS_2. By replacing the bottom MoS_2 layer with the HOPG bilayer, the n-type doping recovers at the step. The step regions show higher sensitivity to the substrate difference than the bulk areas do, indicative of more effective bandgap modulation by edge-terminations under the continuous MoS_2 step junction. Second, the geometries of the continuous steps may not be the only factor for bandgap adjustments. Shin *et al.* have reported that corrugations and HOPG-induced steps in TMDC flakes result in reduced bandgap widths of the TMDCs due to lattice distortion.[28] Nevertheless, neither of the band alignment in Figs. 3 and 4 shows prominent shrinkage of the gap widths. One possible reason for the bandgap discrepancy between HOPG-induced MoS_2 steps in our results and the work of Shin *et al.* is the difference in sample preparation and, thus, different edge conditions.[28] Directly grown on the HOPG substrates right after cleavage using the CVD method, the step edges under MoS_2 layers are cleaner than the transferred cases. At the top left corner in Fig. 4(a), it can be seen that the HOPG step edge is decorated by adsorbates but the step covered by monolayer MoS_2 remains clean. The adsorbates could change interactions such as screening effects and hybridization between MoS_2 and the step edges, influencing the electronic properties of the junctions.[29] The absence of bandgap reduction at both types of continuous MoS_2 steps suggests that in addition to the strain effects, interactions between the top MoS_2 flakes and the bottom layer edges should be considered and worthy of further investigation.

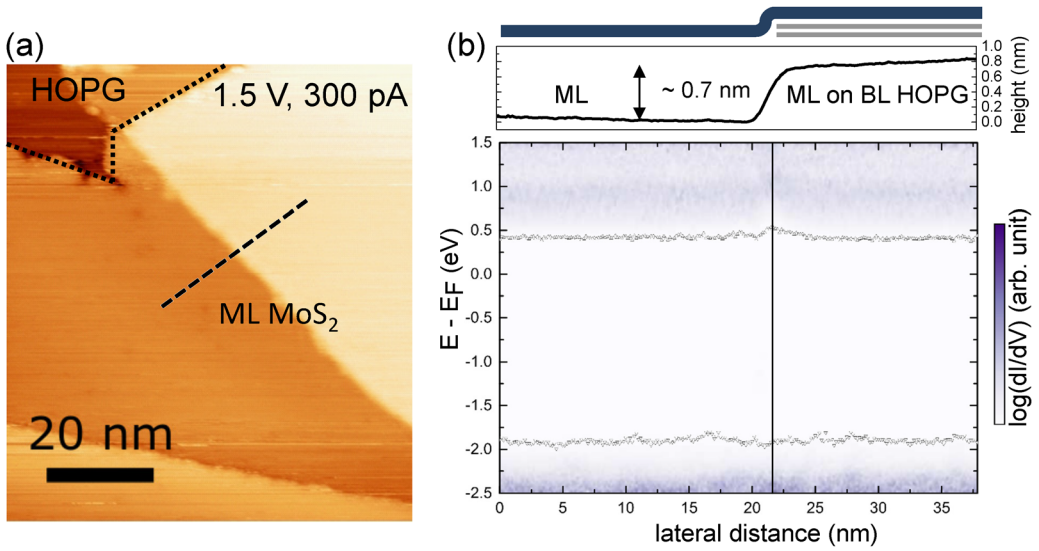

FIG. 4. (a) An STM image of monolayer MoS_2 on a bilayer HOPG step. The dotted line in the top-left corner marks the MoS_2 boundary. (b) An STS band diagram taken along the dashed line in the middle of (a). A height profile and a schematic illustration of the probed area are also presented. Both the fitted CBM and VBM remain nearly constant. The black vertical line indicates the step location in the diagram.

It is also worth noting that in the continuous bilayer–monolayer MoS_2 junction, the CBM varies smoothly from the bilayer to monolayer MoS_2 while the VBM drops quickly. On the one hand, the resemblance between drops of the VBM in Figs. 1 and 3 suggests influences of the in-gap states at the bottom layer edges on the top layer. On the other hand, it is known that the CBM and VBM are both located at K points in monolayer MoS_2; the latter, however, changes to the Γ point in bilayer MoS_2. As a result, Fig. 3 may reflect different origins of band alignment for the valence bands and conduction bands in continuous bilayer–monolayer MoS_2.

In summary, using STM and STS, continuous lateral heterostructures composed of bilayer and monolayer MoS_2 are resolved at the nanoscale. The bandgap moves to a higher energy position without reduction in widths, which, nevertheless, occurs in discontinuous step junctions. Replacing the bottom layer MoS_2 by a bilayer HOPG step suppresses the bandgap variation at the steps. Our discoveries in the thickness-modulated lateral heterojunctions introduce the importance of continuous steps, which should be distinguished from the conventional discontinuous type. The npn-like band alignment allows quantum-wire-like behaviors in the valence band and facilitates the electronic and optoelectronic designs of TMDC-based junctions.[30,31] Investigations of bottom step choices, such as SiO_2 and hexagonal boron nitride, can be carried out for junction modifications in devices. Combined with TMDC stacking techniques, the continuous lateral TMDC junctions are expected to expand nano-sized electronics and low-dimensional devices.

See the supplementary material for the topography of multilayer MoS_2 islands and additional STS diagrams of all junction types.

This work was supported by the Ministry of Science and Technology of Taiwan through Grant No. MOST 109-2119-M-002-024.

AUTHOR DECLARATIONS

Conflict of Interest

The authors have no conflicts to disclose.

Author Contributions

Yu-Hsun Chu: Formal analysis (lead); Investigation (lead); Writing – original draft (equal); Writing – review & editing (equal). **Hou-Ju Chen:** Formal analysis (lead); Investigation (lead); Writing – original draft (equal). **Shin-Ye Lee:** Investigation (supporting). **Christopher John Butler:** Investigation (supporting). **Li-Syuan Lu:** Resources (equal). **Han Yeh:** Resources (equal). **Wen-Hao Chang:** Resources (equal). **Minn-Tsong Lin:** Conceptualization (lead); Funding acquisition (lead); Supervision (lead); Writing – original draft (equal); Writing – review & editing (equal).

DATA AVAILABILITY

The data that support the findings of this study are available from the corresponding author upon reasonable request.

REFERENCES

[1]K. S. Novoselov, A. K. Geim, S. V. Morozov, D. Jiang, Y. Zhang, S. V. Dubonos, I. V. Grigorieva, and A. A. Firsov, "Electric field effect in atomically thin carbon films," Science **306**, 666–669 (2004).
[2]K. S. Novoselov, A. K. Geim, S. V. Morozov, D. Jiang, M. I. Katsnelson, I. V. Grigorieva, S. V. Dubonos, and A. A. Firsov, "Two-dimensional gas of massless Dirac fermions in graphene," Nature **438**, 197–200 (2005).
[3]D. Xiao, G.-B. Liu, W. Feng, X. Wu, and W. Yao, "Coupled spin and valley physics in monolayers of MoS_2 and other group-VI dichalcogenides," Phys. Rev. Lett. **108**, 196802 (2012).
[4]Q. H. Wang, K. Kalantar-Zadeh, A. Kis, J. N. Coleman, and M. S. Strano, "Electronics and opto-electronics of two-dimensional transition metal dichalcogenides," Nat. Nanotechnol. **7**, 699–712 (2012).

[5]H. Wang, C. Li, P. Fang, Z. Zhang, and J. Z. Zhang, "Synthesis, properties, and optoelectronic applications of two-dimensional MoS_2 and MoS_2-based heterostructures," Chem. Soc. Rev. **47**, 6101 (2018).
[6]W. Zhu, T. Low, H. Wang, P. Ye, and X. Duan, "Nanoscale electronic devices based on transition metal dichalcogenides," 2D Mater. **6**, 032004 (2019).
[7]C. Liu, H. Chen, S. Wang, Q. Liu, Y.-G. Jiang, D. W. Zhang, M. Liu, and P. Zhou, "Two-dimensional materials for next-generation computing technologies," Nat. Nanotechnol. **15**, 545–557 (2020).
[8]S. Tongay, W. Fan, J. Kang, J. Park, U. Koldemir, J. Suh, D. S. Narang, K. Liu, J. Ji, J. Li, R. Sinclair, and J. Wu, "Tuning interlayer coupling in large-area heterostructures with CVD-grown MoS_2 and WS_2 monolayers," Nano Lett. **14**, 3185–3190 (2014).
[9]J. Xia, Q. Zeng, J. Zhou, W. Zhou, Q. Zhang, J. Yan, Z. Liu, and Z. X. Shen, "Current rectification and asymmetric photoresponse in MoS_2 stacking-induced homojunctions," 2D Mater. **4**, 035011 (2017).
[10]C. Zhang, C.-P. Chuu, X. Ren, M.-Y. Li, L.-J. Li, C. Jin, M.-Y. Chou, and C.-K. Shih, "Interlayer couplings, Moiré patterns, and 2D electronic superlattices in MoS_2/WSe_2 hetero-bilayers," Sci. Adv. **3**, e1601459 (2017).
[11]C. Zhang, M.-Y. Li, J. Tersoff, Y. Han, Y. Su, L.-J. Li, D. A. Muller, and C.-K. Shih, "Strain distributions and their influence on electronic structures of WSe_2–MoS_2 laterally strained heterojunctions," Nat. Nanotechnol. **13**, 152–158 (2018).
[12]X. Liu, I. Balla, H. Bergeron, G. P. Campbell, M. J. Bedzyk, and M. C. Hersam, "Rotationally commensurate growth of MoS_2 on epitaxial graphene," ACS Nano **10**, 1067–1075 (2016).
[13]C. Zhang, Y. Chen, J.-K. Huang, X. Wu, L.-J. Li, W. Yao, J. Tersoff, and C.-K. Shih, "Visualizing band offsets and edge states in bilayer–monolayer transition metal dichalcogenides lateral heterojunction," Nat. Commun. **7**, 10349 (2016).
[14]M. Tosun, D. Fu, S. B. Desai, C. Ko, J. S. Kang, D.-H. Lien, M. Najmzadeh, S. Tongay, J. Wu, and A. Javey, "MoS_2 heterojunctions by thickness modulation," Sci. Rep. **5**, 10990 (2015).
[15]F.-Y. Shih, Y.-C. Wu, Y.-S. Shih, M.-C. Shih, T.-S. Wu, P.-H. Ho, C.-W. Chen, Y.-F. Chen, Y.-P. Chiu, and W.-H. Wang, "Environment-insensitive and gate-controllable photocurrent enabled by bandgap engineering of MoS_2 junctions," Sci. Rep. **7**, 44768 (2017).
[16]Y. Jia, T. K. Stanev, E. J. Lenferink, and N. P. Stern, "Enhanced conductivity along lateral homojunction interfaces of atomically thin semiconductors," 2D Mater. **4**, 021012 (2017).
[17]X. Dong, C. Yan, D. Tomer, C. H. Li, and L. Li, "Spiral growth of few-layer MoS_2 by chemical vapor deposition," Appl. Phys. Lett. **109**, 051604 (2016).
[18]D. J. Trainer, A. V. Putilov, C. D. Giorgio, T. Saari, B. Wang, M. Wolak, R. U. Chandrasena, C. Lane, T.-R. Chang, H.-T. Jeng, H. Lin, F. Kronast, A. X. Gray, X. Xi, J. Nieminen, A. Bansil, and M. Iavarone, "Inter-layer coupling induced valence band edge shift in mono- to few-layer MoS_2," Sci. Rep. **7**, 40559 (2017).
[19]A. Splendiani, L. Sun, Y. Zhang, T. Li, J. Kim, C.-Y. Chim, G. Galli, and F. Wang, "Emerging photoluminescence in monolayer MoS_2," Nano Lett. **10**, 1271–1275 (2010).
[20]Y. L. Huang, Y. Chen, W. Zhang, S. Y. Quek, C.-H. Chen, L.-J. Li, W.-T. Hsu, W.-H. Chang, Y. J. Zheng, W. Chen, and A. T. S. Wee, "Bandgap tunability at single-layer molybdenum disulphide grain boundaries," Nat. Commun. **6**, 6298 (2015).
[21]C. Zhang, A. Johnson, C.-L. Hsu, L.-J. Li, and C.-K. Shih, "Direct imaging of band profile in single layer MoS_2 on graphite: Quasiparticle energy gap, metallic edge states, and edge band bending," Nano Lett. **14**, 2443–2447 (2014).
[22]Y.-H. Chu, L.-H. Wang, S.-Y. Lee, H.-J. Chen, P.-Y. Yang, C. J. Butler, L.-S. Lu, H. Yeh, W.-H. Chang, and M.-T. Lin, "Atomic scale depletion region at one dimensional $MoSe_2$-WSe_2 heterointerface," Appl. Phys. Lett. **113**, 241601 (2018).
[23]Y. L. Huang, Z. Ding, W. Zhang, Y.-H. Chang, Y. Shi, L.-J. Li, Z. Song, Y. J. Zheng, D. Chi, S. Y. Quek, and A. T. S. Wee, "Gap states at low-angle grain boundaries in monolayer tungsten diselenide," Nano Lett. **16**, 3682–3688 (2016).
[24]B. Sachs, L. Britnell, T. O. Wehling, A. Eckmann, R. Jalil, B. D. Belle, A. I. Lichtenstein, M. I. Katsnelson, and K. S. Novoselov, "Doping mechanisms in graphene-MoS_2 hybrids," Appl. Phys. Lett. **103**, 251607 (2013).
[25]P. Willke, M. A. Schneider, and M. Wenderoth, "Electronic transport properties of 1D-defects in graphene and other 2D-systems," Ann. Phys. **529**, 1700003 (2017).
[26]F. Zahid, L. Liu, Y. Zhu, J. Wang, and H. Guo, "A generic tight-binding model for monolayer, bilayer and bulk MoS_2," AIP Adv. **3**, 052111 (2013).
[27]H.-g. Kim and H. J. Choi, "Thickness dependence of work function, ionization energy, and electron affinity of Mo and W dichalcogenides from DFT and GW calculations," Phys. Rev. B **103**, 085404 (2021).
[28]B. G. Shin, G. H. Han, S. J. Yun, H. M. Oh, J. J. Bae, Y. J. Song, C.-Y. Park, and Y. H. Lee, "Indirect bandgap puddles in monolayer MoS_2 by substrate-induced local strain," Adv. Mater. **28**, 9378–9384 (2016).
[29]M. M. Ugeda, A. J. Bradley, S.-F. Shi, F. H. da Jornada, Y. Zhang, D. Y. Qiu, W. Ruan, S.-K. Mo, Z. Hussain, Z.-X. Shen, F. Wang, S. G. Louie, and M. F. Crommie, "Giant bandgap renormalization and excitonic effect in a monolayer transition metal dichalcogenide semiconductor," Nat. Mater. **13**, 1091–1095 (2014).
[30]F. Wu, H. Tian, Y. Shen, Z. Hou, J. Ren, G. Gou, Y. Sun, Y. Yang, and T.-L. Ren, "Vertical MoS_2 transistors with sub-1-nm gate lengths," Nature **603**, 259–276 (2022).
[31]K. W. Lau, Calvin, Z. Gong, H. Yu, and W. Yao, "Interface excitons at lateral heterojunctions in monolayer semiconductors," Phys. Rev. B **98**, 115427 (2018).